

Magnetic Study of Phases in $\text{FeVO}_4\text{-Co}_3\text{V}_2\text{O}_8$ System

N. GUSKOS^a, G. ZOLNIERKIEWICZ^{a,*}, M. PILARSKA^a, J. TYPEK^a, A. BLONSKA-TABERO^b
AND C. AIDINIS^c

^aInstitute of Physics, West Pomeranian University of Technology, Szczecin, al. Piastów 48, 70-311 Szczecin, Poland

^bDepartment of Inorganic and Analytical Chemistry, Faculty of Technology and Chemical Engineering,
West Pomeranian University of Technology, Szczecin, al. Piastów 42, 70-065 Szczecin, Poland

^cDepartment of Electrical Engineering, Ajman University of Science and Technology, P.O. Box 346, Ajman, UAE

Magnetic properties of four $n\text{FeVO}_4/(1-n)\text{Co}_3\text{V}_2\text{O}_8$ samples obtained in reactions between FeVO_4 and $\text{Co}_3\text{V}_2\text{O}_8$ ($n = 0.96, 0.86, 0.84$ and 0.83 , samples designated S1, S3, S4, S5, respectively) have been investigated by DC magnetisation in field cooling and zero-field-cooling modes and EPR. DC magnetic susceptibility showed paramagnetic behavior of all samples in high-temperature range ($T > 20$ K) and transition to antiferromagnetic state at 16–18 K (depending on sample iron content). Additional magnetic freezing at 8 K was registered for S3–S5 samples containing larger amount of cobalt. The Curie–Weiss law in 100–300 K temperature range indicates that Co^{2+} is in the high-spin state ($S = 3/2$). From the parameters of the hysteresis loop observed for the samples it was calculated that 0.58% of all magnetic (Fe^{3+} , Co^{2+}) ions were involved in the ferromagnetic states. EPR spectra of the samples were recorded in high temperature range ($T > 90$ K). The temperature dependence of the spectral parameters (resonance field, linewidth, integrated intensity) suggested the Fe^{3+} high-spin ions coupled by antiferromagnetic interaction and clusters of ions play major role in EPR spectra.

DOI: [10.12693/APhysPolA.132.24](https://doi.org/10.12693/APhysPolA.132.24)

PACS/topics: 75.40.Cx, 75.50.Ee, 76.30.Fc

1. Introduction

Multicomponent vanadates and their polymorphic modifications, due to their strong and selective catalytic properties in, e.g. oxidative dehydrogenation of the saturated to unsaturated compounds, are intensively studied by different techniques, including electron paramagnetic resonance (EPR) [1–9]. From the point of view of desired catalytic properties, the vanadates containing in their structure chains of face-sharing metal octahedra and isolated VO tetrahedral are especially useful. Thus the $\text{FeVO}_4\text{-Co}_3\text{V}_2\text{O}_8$ system containing also two strong magnetic ions seems to be a promising new catalyst.

A comprehensive study of phases formed in the $\text{FeVO}_4\text{-Co}_3\text{V}_2\text{O}_8$ system in the whole range of compounds concentrations has shown existence of two interesting phases: the howardevansite-type structure (H-type phase) and the lyonsite-type structure (L-type phase) [10]. In H-type structure an edge sharing octahedral dimers of iron are found. In L-type structure the oxygen framework creates three different sites for Fe cation: face-shared octahedral sites, edge/corner-shared octahedral sites and edge-shared trigonal prismatic sites, while Co and V ions occupy two types of isolated tetrahedral sites within the framework [11]. The two end compounds in the $\text{FeVO}_4\text{-Co}_3\text{V}_2\text{O}_8$ system have themselves very interesting physical properties: FeVO_4 is a low symmetry magnetic system undergoing antiferromagnetic (AFM) phase transi-

tion at $T_N = 20$ K, while $\text{Co}_3\text{V}_2\text{O}_8$ displays a complex magnetic order in two-dimensional kagome staircase lattice [12, 13].

Magnetic properties of selected compounds from $\text{FeVO}_4\text{-Co}_3\text{V}_2\text{O}_8$ system were previously studied [1, 2]. The EPR spectra of twenty samples from $\text{FeVO}_4\text{-Co}_3\text{V}_2\text{O}_8$ system at room temperature (RT) were measured and analyzed [1]. Taking into account the g -factors and linewidths, all samples were divided into three groups. In the first group a strong EPR signal was produced by Fe^{3+} residing in FeVO_4 , in the second much weaker EPR spectra were attributed to Fe^{3+} in H-type phase, and in the third ascribed to clusters of small sizes containing Fe and Co ions located in L-type phase. The results of EPR and magnetisation measurements of only two samples: one containing a single H-type phase and the other being the mixture of H-type and L-type phases were presented in [2]. Both samples showed behavior similar to frustrated antiferromagnets [14, 15]. In the high temperature range a very strong atomic force microscope (AFM) interaction was observed in both samples, but competition between magnetic ions (Fe^{3+} and Co^{2+}) located in different sublattices prevented formation of a global magnetic order (magnetic frustration effect). Figure 1 illustrates what has already been accomplished and what is investigated in this paper.

The aim of the present study is to examine the dynamic and static magnetic properties of the four samples from the $\text{FeVO}_4\text{-Co}_3\text{V}_2\text{O}_8$ system. As the numbering of samples presented in Ref. [10] (samples were numbered 1–24) will be continued in this paper (the source of the used samples is the same), the measured samples will be designated as S1, S3, S4, and S5 (they were numbered

*corresponding author; e-mail:
grzegorz.zolnierkiewicz@zut.edu.pl

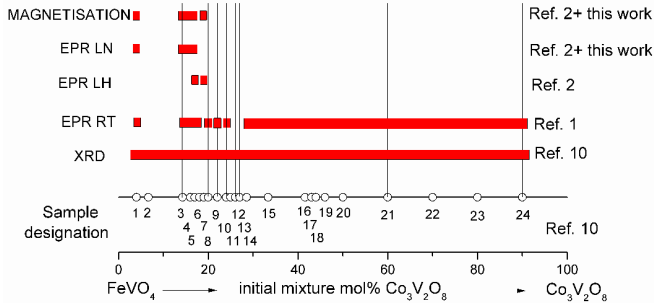


Fig. 1. Schematic presentation of studies carried out on samples from the $\text{FeVO}_4\text{-Co}_3\text{V}_2\text{O}_8$ system. EPR RT, LN, and LH denote EPR measurements made at room temperature (290 K), liquid nitrogen temperature (77 K) and liquid helium temperature (4 K), respectively.

correspondingly as 1, 3, 4, and 5 in [10]). This work is a further step towards full magnetic characterisation of all samples synthesized in the $\text{FeVO}_4\text{-Co}_3\text{V}_2\text{O}_8$ system.

2. Experimental

Synthesis of the investigated four samples is described in Ref. [10]. Final calcination temperatures were 780 °C for samples S1, S3, S4, and up to 840 °C for S5 samples. Diffraction patterns were obtained using the diffractometer PANalytical Empyrean II with Cu radiation. The initial components and the phases determined by X-ray diffraction (XRD) measurements in each sample are listed in Table I. DC magnetization measurements were carried out using an MPMS-7 SQUID magnetometer in 2–300 K temperature range and magnetic fields up to 70 kOe in the zero-field-cooling (ZFC) and field cooling (FC) modes. The EPR spectra were recorded using a standard X-band Bruker E 500 spectrometer ($\nu = 9.45$ GHz) with magnetic field modulation of 100 kHz. The measurements were performed in 90–290 K temperature range using an Oxford helium-flow cryostat.

TABLE I

Chemical composition and XRD detected phase content of the samples.

Sample	Initial mixture [mol%]		XRD detected phase
	FeVO_4	$\text{Co}_3\text{V}_2\text{O}_8$	
S1	96.00	4.00	FeVO_4 + H-type
S3	85.72	14.28	
S4	84.00	16.00	
S5	83.00	17.00	H-type

3. Results and discussion

Figure 2 presents the XRD patterns of all four samples. Sample S5 (Fig. 2a) is monophasic and contains the H-type phase with the formula $\text{Co}_{2.616}\text{Fe}_{4.256}\text{V}_6\text{O}_{24}$, as well as trace amounts of FeVO_4 . In samples S3 and

S4 (Fig. 2b and c), besides the H-type phase, relatively small amounts of iron(III) orthovanadate(V) (marked as *) have been identified, but FeVO_4 content in sample S3 is a little higher than in sample S4. Iron(III) orthovanadate(V) is then the main phase present, besides the H-type phase, in sample S1 (Fig. 2d).

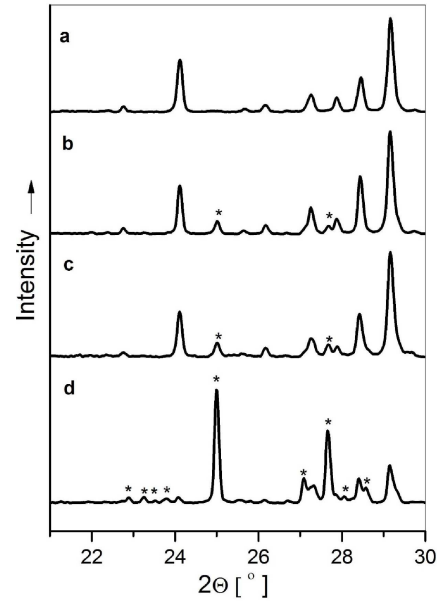


Fig. 2. XRD patterns of sample S5 containing only H-type phase (curve a) and samples S1, S3 and S4 containing H-type phase and FeVO_4 marked as * (curves b, c and d).

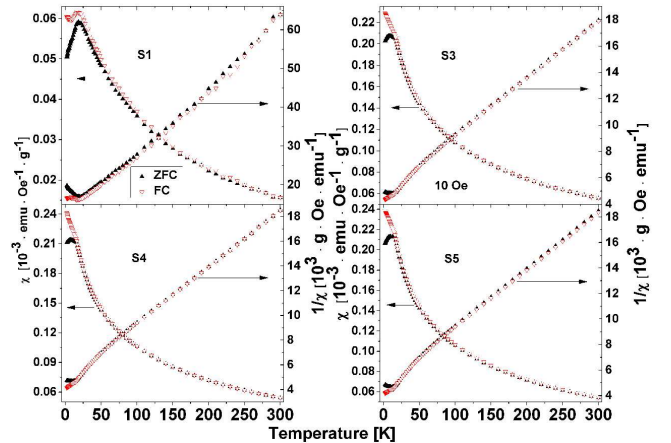


Fig. 3. Temperature dependence of the dc magnetic susceptibility χ (left axis) and the inverse magnetic susceptibility χ^{-1} (right axis) of the four samples registered in an external magnetic field $H = 10$ Oe.

Figures 3 and 4 show temperature dependence of DC magnetic susceptibility χ (left axis) and inverse magnetic susceptibility χ^{-1} (right axis) of all four samples registered at external magnetic fields $H = 10$ Oe and $H = 70$ kOe, respectively. Magnetic susceptibility χ is defined as $\chi = M/H$, where M is magnetisation. With

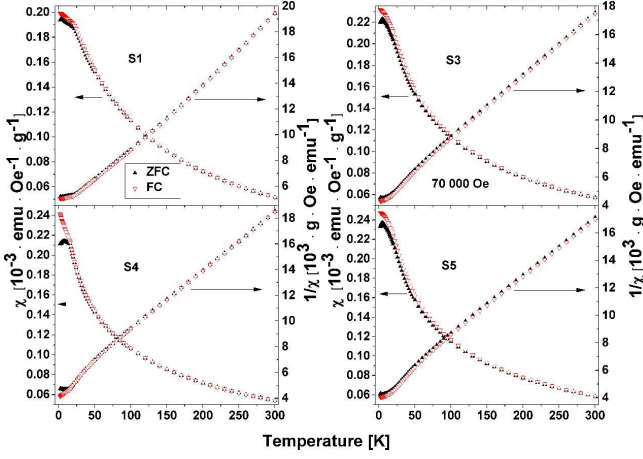


Fig. 4. As in Fig. 3 but for magnetic field $H = 70$ kOe.

exception of S1, other samples showed in the high temperature range ($T > 100$ K) a linear dependence of χ^{-1} on temperature, thus $\chi(T)$ could be described by the Curie–Weiss law

$$\chi(T) = \frac{C}{T - T_{CW}}, \quad (1)$$

where C is the Curie constant, and T_{CW} is the Curie–Weiss temperature. Values of C and T_{CW} calculated using Eq. (1) for samples S3, S4, and S5 are listed in Table II. The measurements of magnetic susceptibility were carried out in magnetic field $H = 70$ kOe in FC and ZFC modes. In ZFC mode the value of C for each sample is a little larger than in FC mode. The negative sign of T_{CW} and its large absolute value indicates a very strong AFM interaction between magnetic ions in the paramagnetic phase. This interaction should lead to the formation of AFM state at low temperatures and indeed the low temperature part ($T < 20$ K) of $\chi(T)$ indicates transition to that magnetic phase. Knowledge of the molar Curie constant C_{mol} allows to calculate the effective magnetic moment (in units of the Bohr magnetons):

$$\mu_{eff} = \sqrt{\frac{3k_B C_{mol}}{N_A \mu_B^2}} \cong 2.828 \sqrt{C_{mol}}, \quad (2)$$

where k_B is the Boltzmann constant, N_A is the Avogadro constant, and μ_B is the Bohr magneton [16]. As our samples (with exception of sample S5) contain at least two different phases with unknown relative concentration, instead of usually used formula unit (f.u.), the exactly known initial mixture unit (i.m.u.) is used. The mass of i.m.u. is calculated simply as

$$m [\text{i.m.u.}] = x \cdot m [\text{FeVO}_4] + (1 - x) \cdot m [\text{Co}_3\text{V}_2\text{O}_8], \quad (3)$$

where x is the molar fraction of mol.% of FeVO_4 in an initial mixture ($0 < x < 1$). The Curie constant can be recalculated using, instead of a gram, the mass of i.m.u. Subsequent application of Eq. (2) yields the effective magnetic moment of i.m.u. representing the magnetic

TABLE II

Parameters extracted from the Curie–Weiss law (Eq. (1)) and the effective magnetic moment of the investigated samples calculated from Eq. (2). The susceptibility was measured in magnetic field $H = 70$ kOe. The magnetic moment (in Bohr magnetons) of an i.m.u. is shown in the last column.

Sample	Mode	T_{CW} [K]	C [$\frac{\text{emu K}}{\text{g Oe}}$]	$\mu_{eff}^{(exp)}$ [$\frac{\mu_B}{\text{i.m.u.}}$]
S3	ZFC	-103.75	0.0231	6.13
	FC	-99.42	0.0229	6.11
S4	ZFC	-102.83	0.0228	6.16
	FC	-101.34	0.0227	6.15
S5	ZFC	-108.88	0.0239	6.34
	FC	-105.31	0.0238	6.33

moment calculated for x iron ions and $3(1 - x)$ cobalt ions (see last column in Table II). Comparing the values of μ_{eff} for different samples, it can be seen that the magnetic moment increases with the increase of $\text{Co}_3\text{V}_2\text{O}_8$ concentration in an initial mixture and thus with the increase of H-type phase. Although the magnetic moment of a single Fe^{3+} ion ($S = 5/2$, $\mu = g\mu_B\sqrt{S(S+1)} \approx 5.9\mu_B$) is larger than a single Co^{2+} ion in ($S = 3/2$, $\mu \approx 3.9\mu_B$), there will be more Co^{2+} ions than Fe^{3+} ions in samples labeled by larger numbers (e.g., S4 and S5). To estimate the contribution of Co ions to the experimental μ_{eff} , the following equation was applied:

$$\mu_{eff} = \sqrt{x\mu_{1eff}^2 + 3(1-x)\mu_{2eff}^2}, \quad (4)$$

where μ_{1eff} is an effective moment of Fe ion, and μ_{2eff} is an effective moment of Co ion (in units of μ_B) [17].

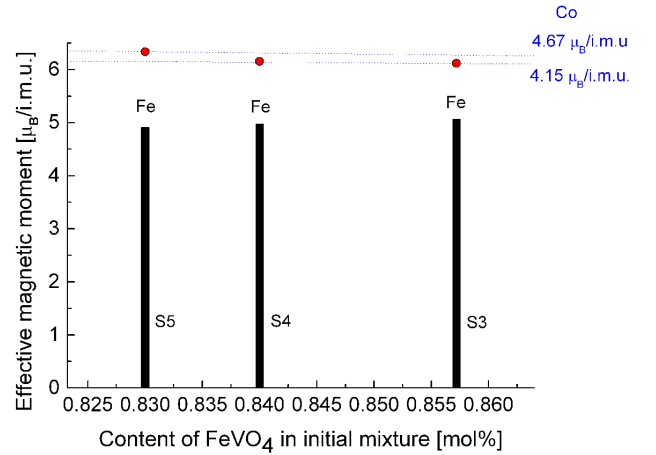


Fig. 5. Measured effective magnetic moment (filled circle) of S3, S4 and S5 samples decomposed into contributions from Fe and Co ions.

In Fig. 5 the measured μ_{eff} of S3, S4 and S5 samples was decomposed into contributions from Fe and Co ions. It was assumed that Fe^{3+} ion is in the high-spin state ($S = 5/2$) with magnetic moment of $5.9 \mu_B$ and the remaining magnetic moment was attributed to Co ion. Cobalt may be in the low-spin state $S = 1/2$ ($\mu \approx 1.7\mu_B$)

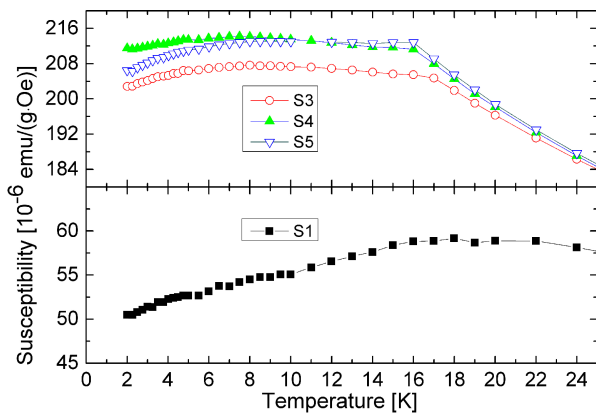


Fig. 6. Temperature dependence of magnetic susceptibility in ZFC mode in low temperature range measured in magnetic field $H = 10$ Oe.

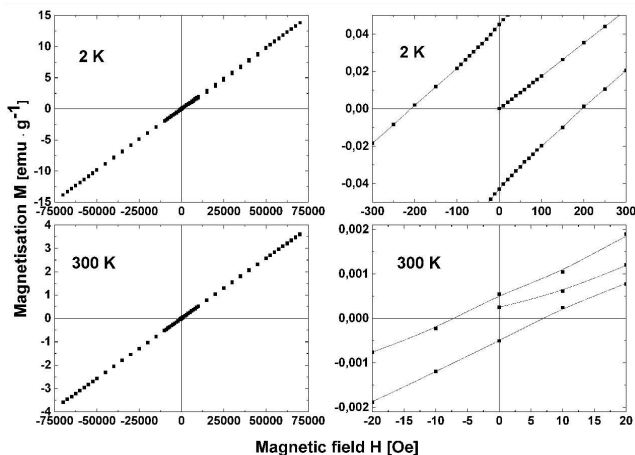


Fig. 7. Isothermal magnetisation of sample S1 at 2 K (left part, top) and 300 K (left part, bottom). Right part shows in an extended scale the central part of hysteresis loops.

or high-spin state $S = 3/2$ ($\mu \approx 3.9\mu_B$). From Fig. 5 it is clearly seen that Co^{2+} ion in our samples is most probably in the high-spin state as each cobalt ion should contribute $4.1\text{--}4.7 \mu_B$ ($g = 2$ assuming) to the observed μ_{eff} . There are two possible additional contributions to such high μ_{eff} of Co^{2+} ion: orbital ($L \neq 0$) magnetic moment (often found for that ion in many matrices) and clustering of Co^{2+} ions. The later could be reasoned using van Vleck formulae for a cluster containing n ions

$$\chi_M = \frac{Ng^2\beta^2}{3nkT} \frac{\sum_S S(S+1)(2S+1)e^{-E(J,S)/kT}}{\sum_S (2S+1)e^{-E(J,S)/kT}}, \quad (5)$$

where n is the number of ions in the cluster [18]. From this formula it is seen that the magnetic moment of a cluster containing n ions is higher than the sum of magnetic moments of n individual, non-interacting ions.

Figure 6 displays temperature dependence of magnetic susceptibility in ZFC mode in the low temperature range measured in an external magnetic field $H = 10$ Oe. Comparison of data susceptibility for four samples in that temperature range shows that sample S1 has significantly

smaller (roughly four times) than other three samples. As the main difference between these samples is the content of $\text{Co}_3\text{V}_2\text{O}_8$ phase, it can be inferred that small amount of cobalt ions in sample S1 (roughly four times smaller) is the main reason of the reduced χ value. Concerning the shape of $\chi(T)$, there are two distinct temperatures at which a kink and a local maximum are observed. In all four samples in 16–18 K temperature range a marked change in value of $d\chi/dT$ is noticeable (the slope of $\chi(T)$ is steeper at higher temperatures and more flat at lower temperatures). Since in a single crystal of FeVO_4 in this temperature range a transition to AFM phase has been detected, that observed kink in $\chi(T)$ dependence may be interpreted as the evidence of this transition. In S3, S4 and S5 samples a shallow maximum in $\chi(T)$ is visible at temperature ≈ 8 K, but not in S1 sample. Considering the phase content of our samples it is presumed that this maximum is due to cobalt ions. There are only insignificant amounts of these ions (and also H-type phase) in S1 sample and this explains the lack of a susceptibility maximum close to 8 K. Freezing of spins (mostly cobalt ions in H-type structure) might be the reason of diminishing susceptibility at temperatures below 8 K.

TABLE III

Parameters of the hysteresis loop (H_c — coercive field, M_r — remanence) measured at $T = 2$ K together with the magnetic moment (in Bohr magnetons) of an i.m.u.

Sample	H_c [Oe]	M_r [emu/g]	M_r [μ_B /i.m.u.]
S1	201	0.0439	0.0323
S3	476	0.1202	0.0366
S4	499	0.1291	0.0373
S5	654	0.1943	0.0378

Figure 7 shows isothermal magnetisation $M(H)$ of sample S1 at 2 and 300 K. At both temperatures $M(H)$ is almost a linear function, except in weak magnetic fields. Right part in Fig. 7 displays in an extended scale the central part of $M(H)$ dependence in which a familiar shape of the hysteresis loop could be recognized. The linear part of $M(H)$ at 300 K is expected for a material in paramagnetic phase. The values of parameters of the hysteresis loop (H_c — coercive field, M_r — remanence) for all samples measured at $T = 2$ K are presented in Table III. The appearance of hysteresis loop in isothermal magnetisation indicates the presence of the ferromagnetic (FM) component in all four samples. From Table III follows that the coercive field increases with the cobalt content as do the remanence expressed as the Bohr magnetons on the initial mixture unit (i.m.u.). The last quantity allows to estimate the percentage of magnetic ions (Fe, Co) involved in an FM component at 2 K. If an average value of M_r for all samples is taken as $0.036 \mu_B$ /i.m.u. and an average effective magnetic moment as $6.2 \mu_B$ /i.m.u., than only $(0.036/6.2)100 = 0.58\%$ of all magnetic ions form FM state.

It is very probable that the origin of the FM loop and thus the FM phase is extrinsic to the investigated mate-

rial. Very small amount of magnetic ions involved in this phase suggests the presence of an unintentional admixture of a phase that is already FM at RT. Iron oxides, especially magnetite Fe_3O_4 , can easily fulfill this requirement. They will be difficult to detect in XRD measurements due to their low content. As the observation of FM loop at RT excludes the existence of low temperature superparamagnetic phase (the blocking temperature would be higher than RT), this admixture phase is expected to form magnetic domains much larger than nanometric in sizes.

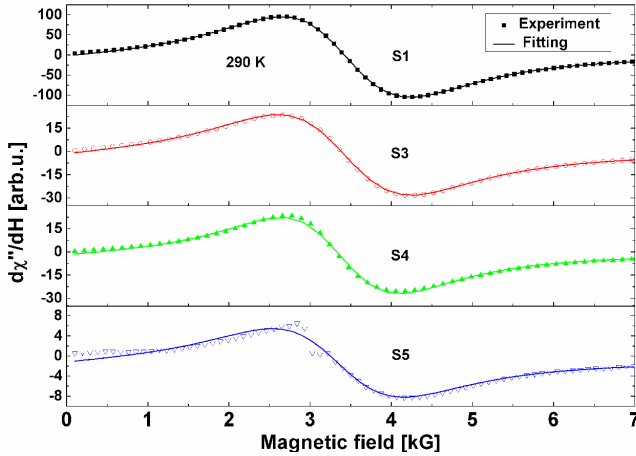


Fig. 8. Experimental (symbols) and fitted (lines) magnetic resonance spectra of the four samples registered at $T = 290$ K.

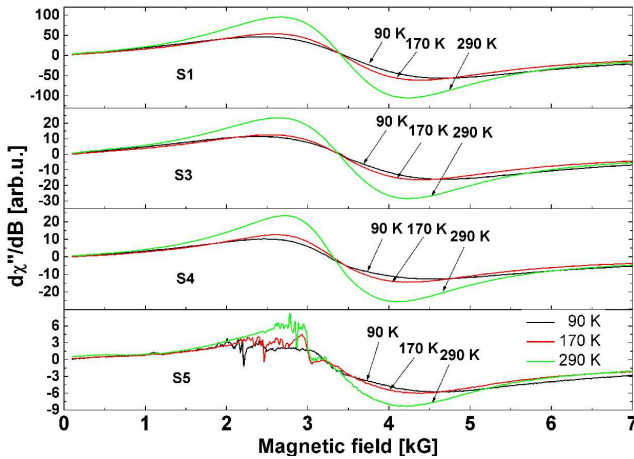


Fig. 9. Experimental magnetic resonance spectra of the four samples at different temperatures.

Results of EPR measurements in 90–300 K range are presented in Figs. 8–10. EPR spectra of all samples are similar in appearance — they consist of a broad line of Lorentzian line shape. In Fig. 8 the EPR experimental and fitted spectra of the four samples recorded at $T = 290$ K are shown. The fittings gave satisfactory results and allowed to obtain the values of the resonance field, linewidth and signal amplitude for each registered

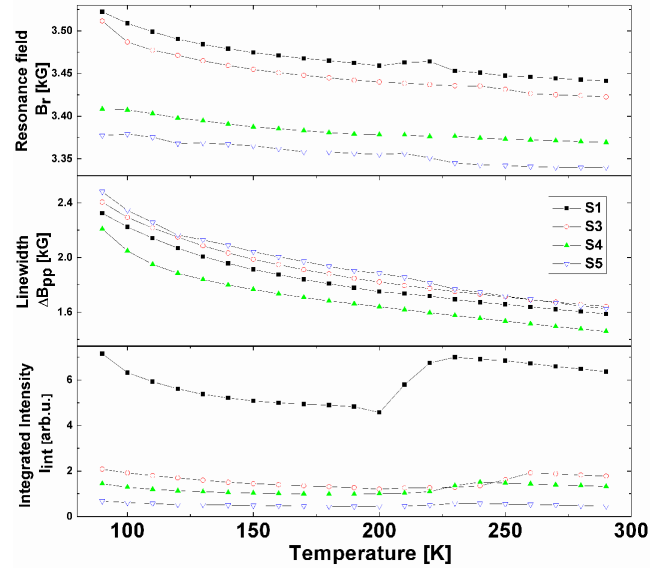


Fig. 10. Temperature dependence of magnetic resonance spectra: resonance field (top part), linewidth (middle part), integrated intensity (bottom part).

temperature. As an example, experimental EPR spectra of the four samples at three different temperatures are shown in Fig. 9. Generally, the smaller the amount of Fe ions in a sample, the weaker the EPR spectrum. Thus the EPR spectrum of sample S5 is much weaker than of S1. This indicates that Fe^{3+} ions play a dominant role in the formation of EPR spectra in our samples.

As the EPR spectrum of sample S5 is rather weak, additional magnetic components, having a small concentration, become noticeable on the background of a dominating broad Fe^{3+} line. This is clearly visible in Fig. 9, bottom part, where many narrow lines are evident in 2–3 kG range. They are most probably not arising from the high-spin Co^{2+} ions as these are usually observed only at liquid helium temperatures due to a very fast spin–lattice relaxation time. As the observed lines are narrow they must be produced by magnetic species weakly connected with the dominating population of strongly interacting Fe^{3+} ions and with the crystal lattice. In fact they should be treated as magnetic defects associated with structural defects appearing on grain and phase boundaries. It could be speculated that their magnetism is due to the presence of iron and cobalt ions forming nanometric size clusters.

Figure 10 presents the temperature dependence of EPR parameters obtained from fitting of Lorentzian line and also the integrated intensity, calculated as the product of amplitude and square of linewidth, $I_{int} = A\Delta B^2$. I_{int} is an important parameter, which is proportional to the magnetic susceptibility of the spin system involved in formation of EPR spectrum at microwave frequency [19]. It would be interesting to compare $I_{int}(T)$ obtained from EPR measurements with the static magnetic susceptibility $\chi(T)$ acquired previously from magnetisation study. Temperature dependence of $\chi(T)$ in 100–300 K range was

very well described by the Curie–Weiss law (except for sample S1), while $I_{int}(T)$ shows more complicated thermal behavior (Fig. 10, bottom part). There is a local maximum in $I_{int}(T)$ plot for all samples in 230–260 K range. This maximum is especially evident in samples with large amount of iron ions, because the local maximum values in I_{int} are 7.0, 1.9, 1.5, and 0.6 for samples S1, S3, S4, and S5, respectively. This local maximum may arise from the iron clusters having an AFM $S = 0$ ground state and the excited $S \neq 0$ states. At low temperatures ($T < 200$ K) the excited magnetic states are not populated, so there is no EPR signal from the clusters in that range. The presence of AFM iron clusters has been manifested itself in S1 sample as the lack of the Curie–Weiss behavior in $\chi(T)$ at high temperatures (see Figs. 3 and 4). Below 200 K the function $I_{int}(T)$ is roughly approximated by the Curie–Weiss law with an AFM (negative) T_{CW} constant. Thus the EPR signal in 90–300 K range in the four samples is arising from the two spin subsystems: (i) paramagnetic Fe^{3+} ions subjected to AFM interaction and (ii) AFM spin clusters that manifests themselves only at high temperatures.

4. Conclusions

Magnetisation studies and EPR spectroscopy have revealed a complicated picture of magnetic properties of the four samples from the $\text{FeVO}_4\text{-Co}_3\text{V}_2\text{O}_8$ system containing two magnetic ions (Fe^{3+} and Co^{2+}). At high temperatures, $T > 100$ K, the main magnetic component is paramagnetic with strong AFM interactions. They involve both kinds of magnetic ions, each in the high-spin state. The secondary magnetic components are AFM spin clusters, containing mostly iron ions. They are active in EPR spectrum in high-temperature range, $T > 200$ K. The observed hysteresis loop indicates the presence, although in small amounts, of FM component and its origin is probably extrinsic (iron oxides). At low temperatures transition to AFM phase is observed (in 16–18 K range) and another transition (≈ 8 K) believed to be due to the spin freezing in H-type phase. Occurrence of FM and AFM features imply competition of magnetic interactions in $\text{FeVO}_4\text{-Co}_3\text{V}_2\text{O}_8$ system, leading to a frustrated magnetic structure. This is not surprising considering the nature of the investigated system with multiple phases and with two strong magnetic ions (Co and Fe) as well as a very complicated crystal structure of the involved constituents.

References

- [1] N. Guskos, G. Zolnierkiewicz, J. Typek, A. Blonska-Tabero, *Physica B* **406**, 2163 (2011).
- [2] N. Guskos, G. Zolnierkiewicz, J. Typek, R. Szymczak, A. Guskos, P. Berczynski, A. Blonska-Tabero, *Mater. Sci.-Pol.* **31**, 601 (2013).
- [3] N. Guskos, V. Likodimos, S. Glenis, G. Zolnierkiewicz, J. Typek, R. Szymczak, A. Blonska-Tabero, *J. Appl. Phys.* **101**, 103922 (2007).
- [4] G. Zolnierkiewicz, N. Guskos, J. Typek, E.A. Anagnostakis, A. Blonska-Tabero, M. Bosacka, *J. Alloys Comp.* **471**, 28 (2009).
- [5] N. Guskos, H. Ohta, G. Zolnierkiewicz, S. Okubo, W.-M. Zhang, J. Typek, C. Rudowicz, R. Szymczak, M. Bosacka, T. Nakamura, *J. Non-Cryst. Solids* **355**, 1419 (2009).
- [6] J. Typek, G. Zolnierkiewicz, N. Guskos, R. Szymczak, A. Blonska-Tabero, *Rev. Adv. Mater. Sci.* **23**, 207 (2010).
- [7] J. Typek, G. Zolnierkiewicz, M. Bobrowska, N. Guskos, A. Blonska-Tabero, *Solid State Sci.* **34**, 31 (2014).
- [8] A. Bezkrvnyi, N. Guskos, J. Typek, N.Yu. Ryabova, M. Bosacka, A. Blonska-Tabero, M. Kurzawa, I. Rychlowska-Himmel, G. Zolnierkiewicz, *Mater. Sci.-Pol.* **23**, 883 (2005).
- [9] N. Guskos, A. Bezkrvnyi, J. Typek, N.Yu. Ryabova, A. Blonska-Tabero, M. Kurzawa, M. Maryniak, *J. Alloys Comp.* **391**, 20 (2005).
- [10] A. Blonska-Tabero, M. Kurzawa, *J. Therm. Anal. Calorim.* **88**, 33 (2007).
- [11] X. Wang, D.A. Vander Griend, C.L. Stern, K.R. Poeppelmeier, *Inorg. Chem.* **39**, 136 (2000).
- [12] B. Bojanowski, S. Kaczmarek, *Mater. Sci.-Pol.* **32**, 188 (2014).
- [13] Y. Chen, J.W. Lynn, Q. Huang, F.M. Woodward, T. Yildirim, G. Lawes, A.P. Ramirez, N. Rogado, R.J. Cava, A. Aharony, O. Entin-Wohlman, A.B. Harris, *Phys. Rev. B* **74**, 014430 (2006).
- [14] H. Martinho, N.O. Moreno, J.A. Sanjurjo, C. Rettori, A.J. García-Adeva, D.L. Huber, S.B. Oseroff, W. Ratcliff II, S.-W. Cheong, P.G. Pagliuso, J.L. Sarrao, G. B. Martins, *Phys. Rev. B* **64**, 024408 (2001).
- [15] J. Lin, P. Tong, D. Cui, C. Yang, J. Yang, S. Lin, B. Wang, W. Tong, L. Zhang, Y. Zou, Y. Sun, *Sci. Rep.* **5**, 7933 (2015).
- [16] R.J.D. Tilley, *Perovskites: Structure-Property Relationships*, Wiley, Chichester 2016.
- [17] E.I. Kondorskii, O.S. Galkina, L.V. Lazareva, *JETP Lett.* **30**, 656 (1979).
- [18] L. Sorace, D. Gatteschi, in: *Inorganic and Bio-Inorganic Chemistry*, Vol. 1, Ed. I. Bertini, Eolss Publ., Oxford 2009, p. 199.
- [19] S.V. Demishev, A.V. Semeno, N.E. Sluchanko, N.A. Samarin, A.A. Pronin, Y. Inogaki, S. Okubo, H. Ohta, Y. Oshima, L.I. Leonyuk, *Phys. Solid State* **46**, 2238 (2004).